Current collectors corrosion behaviours and rechargeability of TiO2 in Aqueous Electrolyte Aluminium-ion batteries

Burcu Unal, Ozlem Sel, Rezan Demir-Cakan

Current Collectors Corrosion Behaviours and Rechargeability of TiO_2 in Aqueous Electrolyte Aluminium-ion Batteries

Burcu Unal[a,b], Ozlem Sel[c,d] and Rezan Demir-Cakan[a,b]*

[a] Department of Chemical Engineering, Gebze Technical University, Gebze, Kocaeli, 41400, Turkey

[b] Institute of Nanotechnology, Gebze Technical University, Gebze, Kocaeli, 41400, Turkey

[c] Chimie du Solide et de l'Energie, UMR 8260, Collège de France, 11 Place Marcelin Berthelot, 75231 Paris Cedex 05, France

[d] Réseau sur le Stockage Electrochimique de l'Energie (RS2E), CNRS FR 3459, 33 Rue Saint Leu, 80039 Amiens Cedex, France

*Corresponding author: demir-cakan@gtu.edu.tr

Abstract

The effects of current collectors on the battery performance have significant role, especially in aqueous electrolyte Al-ion batteries, as corrosion effects lead to rapid capacity degradation over cycles. To overcome this problem, we present a study investigating the selection of suitable current collectors and their impact on battery performance. Four different current collectors are selected for this purpose: stainless steel (**SS**), nickel foil (**Ni**), titanium foil (**Ti**) and graphite plate (**GP**). It has been proven by corrosion tests, cyclic voltammetry and charge-discharge studies that **GP** is the best current collector by minimizing the corrosion effect and H_2 evolution reaction (HER). The anatase phase TiO_2 used with **GP** current collector provides a 249 mAh g^{-1} initial discharge capacity at a current density of 3A g^{-1}, while inferior or no electrochemical activity is observed with **Ti**, **SS**, **Ni** current collectors. The observations here provide insights into the selection of corrosion-resistant current collectors to achieve stable battery performance in the field of aqueous electrolyte Al-ion batteries.

Keywords: Aqueous electrolyte, Al-ion battery, current collector, corrosion, TiO_2

1. Introduction

Currently, Li-ion batteries (LIBs) dominate the marketplace for portable devices or electric vehicles because of their high energy density. While developments in the field of LIB technology continue, there are some concerns regarding the use of highly flammable electrolytes and toxic heavy metals on the cathode side. In addition, the threat of future depletion of lithium reserves has been the driving force for researchers to look for alternative chemistries for energy storage systems (1). As a result, in recent years, Li-ion batteries have gained immense scientific acceptance. As it stands now, the majority of Li-ion batteries are based on various metal ions such as polyvalent metal ions, such as multivalent-metal ions (Zn^{2+}, Mg^{2+}, Ca^{2+}, Al^{3+}) and alkali metal ions (Li^{+}, Na^{+}, K^{+}) (2). Among these, aluminium offers the potential to compete with LIBs, providing relatively low cost, safety, ease of use and ability to allow three electrons transfer (3, 4). At the same time, aluminium is one of the most abundant metals on earth and its gravimetric and volumetric capacities are comparable to Li (theoretical gravimetric and volumetric capacities are 2.98 Ah g^{-1} and 8.04 Ah cm^{-3}, respectively) (5). In addition to that, the ionic radius of Al^{3+} (53.5 pm) is smaller than that of the Li^{+} ionic radius (76 pm) and is therefore a promising candidate when it comes to the intercalation mechanism in energy storage system (6, 7).

In rechargeable Al-ion batteries (AIBs), development of high-capacity electrode materials and investigation of suitable electrolytes are important for performance improvement. AIB studies started more than a decade ago using ionic liquids (ILs) (*i.e.* $AlCl_3$/EMICl (1-ethyl-3-methylimidazolium chloride) electrolytes and aluminium metal as anode (8, 9). These ionic liquid electrolytes initially encouraged the studies since they provide stable electrochemical behaviour and high specific capacity with electrodes. However, chloroaluminate ionic liquid electrolytes have had some challenging issues as they present high cost, moisture sensitivity, and large volume use (10). The transition from ILs electrolyte to aqueous electrolyte, usually prepared using $AlCl_3$, $Al(NO_3)_3$, $Al_2(SO_4)_3$ salts, are better alternatives to IL-based electrolytes due to their cost-effectiveness, higher ionic conductivity, easy preparation without dependence on glove box conditions (11). However, the major disadvantage of aqueous electrolyte (AAIBs) compared to non-aqueous Al-ion batteries is the low energy density resulting from the low thermodynamic stability of water in the narrow potential window (1.23 V) (12). Thus, unlike other aqueous electrolyte metal ion batteries (*e.g.* aqueous zinc ion batteries), due to the low reduction voltage of aluminium (-1.68 V *vs*. SHE), the competitive hydrogen evolution reaction (HER) occurs at the electrode surface (13). Moreover, when aqueous electrolytes are used, the

problem of corrosion in current collectors arises, causing low discharge capacity and Coulombic efficiency. In chloride-rich environments, Cl^- ions react with the metal substrate, penetrating the substrate layer and causing corrosion of current collectors (14). Nevertheless, chloride-based electrolytes have been studied in aqueous Al-ion batteries more often, since sulfate and nitrate-based aqueous electrolytes show either no or very weak electrochemical activity (15). To understand the role of Cl^- ions in the field of AAIBs, Liu *et al.* investigated the use of TiO_2 nanotube electrode by adding NaCl to $Al_2(SO_4)_3$ aqueous electrolyte. They observed that the electrode containing only $Al_2(SO_4)_3$ electrolyte showed no electrochemical activity, while reversible redox peaks were observed with the addition of Cl^-, indicating the role of Cl^- ions in the aqueous electrolyte during the intercalation process (16). In a very recent study, Kumar *et al*. also investigated the role of Cl^- in the diglyme solvent electrolyte (containing $Al(OTf)_3$) in which charge-carrier electrochemical species are generated in the presence of tetrabutylammonium chloride additive, reducing the charge transfer resistance and the surface activation energy of the electrodes (17).

Regarding electrode materials in the field of AAIBs, recently VO_2 (1), V_2O_5 (18), anatase TiO_2 (19-21), graphite (22, 23), copper hexacyanoferrate (CuHCF, Prussian blue analogues, PBAs) (24), conductive polymers (25, 26) or organic compounds (27) have been studied as host electrode materials. Among these electrode materials, the use of TiO_2 as an active material is advantageous because it is non-toxic and has a stable chemistry in which charge carrier ions easily insert and de-insert into/from the structure in a reversible manner (16). In 2012, Liu *et al.* first investigated the Al^{3+} insertion into anatase TiO_2 nanotube arrays anode in 1.0 M $AlCl_3$ aqueous electrolyte as an alternative to Al metal. The TiO_2 film was prepared by anodization on a metallic Ti collector, which provides maximum electron conduction between the anode and the substrate. Furthermore, XPS analysis was performed to understand the mechanism of Al^{3+} ion insertion after the electrode was discharged. While Ti^{4+}/Ti^{3+} reduction from anatase TiO_2 was responsible for the capacity contribution during the Al^{3+} insertion into the TiO_2 structure, Ti^{4+} was irreversibly reduced to Ti^{2+} (454.9 eV in the XPS spectrum) to maintain the charge balance leading to the lower initial Coulombic efficiency (19).

The current collector, another very important cell component, strongly influences electrochemical performance, hence has to be properly selected in the field of Al-based batteries. For instance, Reed and Menke reported that the corrosive current from an unstable current collector could be a misinterpretation of redox reactions (28). Oh *et al.* investigated the stability of current collectors in aluminum chloride containing 1-ethyl-3-methylimidazolium

chloride electrolyte. They have observed that while Ni is electro-chemically and chemically unstable, Mo current collector exhibits fairly stable and reversible redox cycling (29). Later, Lahan *et al.* conducted a study investigating the effect of current collectors on electrochemical activity in aqueous electrolyte system (30). To the best of our knowledge, although there are few studies in the field of Al ion batteries focusing on the behaviour of current collectors, the corrosion behaviour of current collectors and corrosion rate measurements via Tafel polarisation curves and its impact on the electrochemical performance of aqueous electrolyte Al ion batteries have rarely been considered in detail.

In this study, potential current collectors were screened focusing on their corrosion behaviour and electrochemical stability. Four different current collectors were selected for this purpose, namely, stainless steel foil (**SS**), nickel foil (**Ni**), titanium foil (**Ti**) and graphite plate (**GP**). Their electrochemical stability was tested in an aqueous electrolyte containing Al salts by cyclic voltammetry (CV) and potantiodynamic polarization measurements by Tafel extrapolation method. Later, TiO_2, as one of the most promising anodes, was synthesized to further emphasize the effect of current collector performance in 1.0 M $AlCl_3$ aqueous electrolyte.

2. Experimental

2.1. Materials and methods

The titanium (IV) isopropoxide (Sigma Aldrich) was used as a precursor for TiO_2 synthesis. 1.4 ml of titanium (IV) isopropoxide was dispersed in 50 ml of ethanol for two hours at room temperature. This mixture was then added dropwise into 50 ml of deionized water and stirred with a magnetic stirrer for 2 hours. The resulting white precipitate was washed with distilled water and ethanol and dried in an oven at 80 °C overnight. It was then calcined under air at 400 °C for 4 hours to obtain the desired stable crystallographic structure (30).

Morphological characterizations of the current collectors and TiO_2 were investigated by scanning electron microscope (SEM Philips XL30). X-ray diffraction, XRD (Bruker D8 diffractometer 2θ mode, Cu Kα radiation, λ = 1.5406 nm) patterns of the samples were recorded in the range of 2θ = 10-70°. The Scherrer equation for the calculation of the crystallite size and the Bragg equation for the interplanar spacing (d-space) of the synthesized anatase TiO_2 were used using OriginPro Software multiple peak analyzer based on full width at half maximum

(FWHM). TEM/HR-TEM (JEOL JEM 2100F) was used to observe the structure of synthesized TiO_2 particles.

2.2. Electrochemical Measurements

Electrochemical measurements of the bare current collectors **SS** (AISI 316, $Fe/Cr_{18}/Ni_{10}/Mo_3$, 0.05 mm, Goodfellow, France), **Ni** (%99.99, 0.25 mm, Goodfellow, France), **Ti** (ASTM 265, 0.125 mm, Marmara Titanium, Turkey), **GP** (>%99, sheet, 0.55 mm, Graftech, Turkey) were carried out by cyclic voltammetry (CV) in 1.0 M $AlCl_3$ (pH = 2.86) aqueous electrolyte at a 5mV/s sweep rate. These tests were performed in a 3-electrode configuration in beaker cell using platinum as counter electrode and Ag/AgCl (3.5 M KCl) as reference electrode. The electrolyte volume of 10 ml was kept constant in each experiment. The area of the current collectors is 1.0 cm^2.

Both CV measurements and potentiodynamic measurement (linear polarization resistance-LPR) were performed using a Biologic VMP-3 potentiostat and EC-Lab software to investigate the corrosion behaviour of the current collectors. The polarization curves of the current collectors were fitted using the Tafel extrapolation method in the voltage range from 1.0 to -1.0 V at a scan rate of 1 mV s^{-1} in 1.0 M $AlCl_3$ aqueous electrolyte. The scans were started from the negative towards the positive polarization. All experiments were performed at room temperature and in a 3-electrode cell configuration as described above.

After the electrochemical stability of the bare current collectors was determined by CV and LPR, the synthesized TiO_2 active electrode material was tested. The electrodes were prepared using 80% active material, 10% Carbon SP conductive additive and 10% polyvinylidene fluoride (PVDF) binder in N-methyl-2-pyrrolidone (NMP) solvent. Then the electrode slurry was casted onto each current collector (1 cm^2) and dried for 4 h at 60 ^oC. The working electrode contains 1.5 mg of active material with a coating thickness of ~30 μm. Galvanostatic charge-discharge measurements were performed in a 3-electrode cell configuration over an operating voltage range from -1.13 to -0.2 V and a constant current density of 3.0 A/g. An Ag/AgCl (3.5 M KCl, satd' AgCl) electrode was used as reference electrode and graphite as counter electrode in 1.0 M $AlCl_3$ aqueous electrolyte.

3. Results and Discussion

Prior to the electrochemical performance measurements, the pH and conductivity studies were performed to select the appropriate electrolyte. Ionic conductivity and pH measurements of

aqueous electrolytes prepared with various concentrations of aluminium salts ($AlCl_3$, $Al(NO_3)_3$, $Al_2(SO_4)_3$) are given in Supporting Information **Figure S1**. As expected, ionic conductivities are observed to increase with increasing concentration for all three electrolytes. However, the ionic conductivities of the electrolytes containing $AlCl_3$ and $Al(NO_3)_3$ salts are higher and do not show a significant difference, while the ionic conductivity and pH of the $Al_2(SO_4)_3$ electrolyte are much lower. One of the issues is the solubility of $Al_2(SO_4)_3$ at higher concentration, *i.e.*, more than 0.5 M $Al_2(SO_4)_3$, the electrolyte needs to be heated to dissolve and the measurements were performed after cooling at room temperature. Lahan and Das studied the (de)intercalation of Al^{3+} ion in aqueous electrolytes prepared with different Al-salts using MoO_3 electrode (31). They showed that the first discharge capacity of the $Al(NO_3)_3$ containing electrolyte achieved an extraordinary value (such as ~21 Ah g^{-1}) while it causes the cell to fail in the following cycles due to the strong oxidizing nature of the NO^{3-} anion. On the other hand, $AlCl_3$ provided higher Al^{3+} ion storage capacity, long-term stability and greater capacity retention than $Al_2(SO_4)_3$ and $Al(NO_3)_3$ with minimum polarization. It is obvious that the optimisation of electrolyte plays a critical role in the development of rechargeable aqueous electrolyte AIBs and therefore pH also needs to be considered (31). It has been reported that metal oxides such as TiO_2 in acidic media can host H^+ as well as Al^{3+} ion to charge balance at low pH (32) and it is generally accepted that proton (de-)insertion in strongly acidic media (pH≈2) is a common feature of mesoporous TiO_2 films (33). Based on the pH and ionic conductivity effects on the electrochemical performances (*i.e.*, TiO_2), a 1.0 M $AlCl_3$ aqueous electrolyte was chosen for further analysis.

Cyclic voltammetry (CV) tests were performed at a scan rate of 5mV/s in 1.0 M $AlCl_3$ aqueous electrolyte to characterize the electrochemical stability of four different collectors (**GP**, **Ni**, **SS**, **Ti**) (**Figure 1**). **Figure 1 (a-b)** shows that when **Ni** and **SS** current collectors operated in the voltage range (-1.2 - 1.0 V), hydrogen evolution was immediately noticeable on the surface of both current collectors. With the start of the CV, it was clearly seen that the **SS** dissolved/corroded and electrolyte colour became greenish demonstrating that these two current collectors are not suitable for aqueous electrolyte Al-ion battery. According to the CV measurements of the **Ti** and **GP** current collectors in the same voltage range as shown in **Figure 1(c-d)**, both of them demonstrated no degradation and discoloration in the electrolyte. In **Figure 1e**, the CV performances of the 4 current collectors are gathered in a single graph for comparison. The cathodic potential region of the CV curves (marked as dotted lines) were enlarged as insets, which clearly show that **Ti** and **GP** are the most stable among the 4 current

collectors in the desired operating voltage range of (-1.2 - 0.5) V. H_2 formation on current collectors can also be explained by the volcano plot, a useful descriptor of hydrogen evolution activity for various metals, which shows the relationship between the observed exchange current density and hydrogen bond adsorption strength, where the exchange current densities of **SS** and **Ni** are much higher than those of **Ti**, indicating lower H_2 formation on **Ti** current collector, in agreement with literature reports (12, 15).

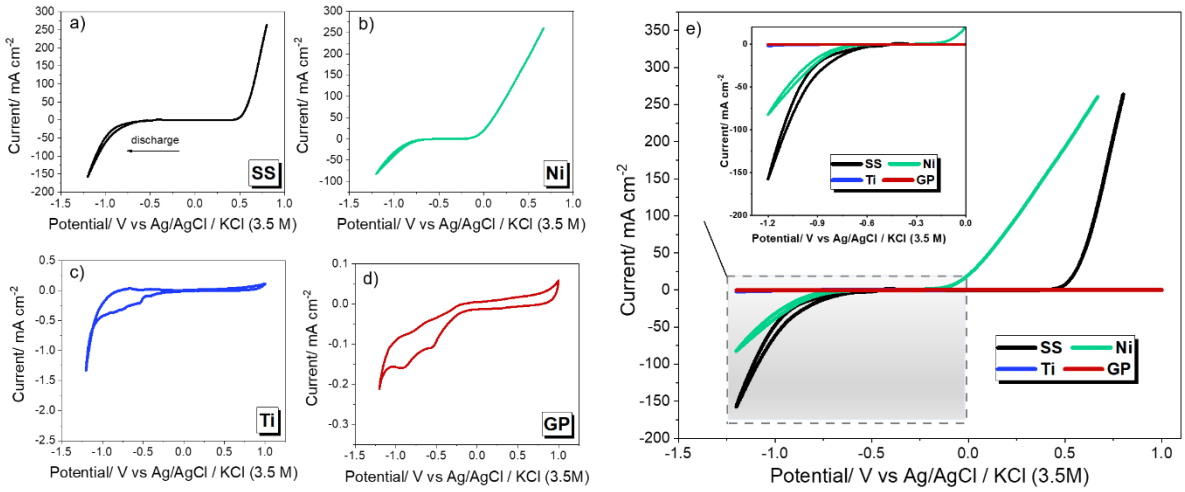

Figure 1. First CV profiles scanned between -1.2 – 1.0 V at 5mV s^{-1} scan rate in 1.0 M $AlCl_3$ of a) **SS**, b) **Ni**, c) **Ti,** d) **GP** current collectors and e) comparison of current collectors.

After the CV measurements, the current collectors were characterized by SEM to detect their morphological changes as shown in **Figure S2**. As supported by the SEM images, cracks are clearly visible on the **SS** and **Ni** surfaces, while minimal changes were observed on the **GP** and **Ti** current collectors. The corrosion behaviour of **Ti**, **Ni**, **SS** and **GP** was investigated in a three-electrode cell configuration in 1.0 M $AlCl_3$ aqueous electrolyte (pH = 2.86). In order to determine the corrosion rate of the current collectors in aqueous electrolyte, polarization curves were obtained by LPR measurements, and the experimentally obtained polarization curves (log |I| *vs.* E_{we}) near the corrosion potential were fitted by applying Tafel extrapolation (**Figure 2**). **SS** current collector started to deteriorate rapidly and dissolved in the electrolyte, causing the electrolyte colour change to light blue/green together with the strong hydrogen evolution reaction (**Figure S3a**). Meanwhile, pitting corrosion also occurred on the **SS** surface in the presence of Cl^- ions in the electrolyte. The main factor causing pitting corrosion is the breakdown of the passivity layer (*i.e.*, oxide film layer on the steel surface) and can also occur

autocatalytically in nature (34-36). Herein, the presence of highly oxidizing agents such as chloride ions has a destructive effect on the electrode, which can be seen in SEM images (**Figure S2)**.

Looking at the **Figure S3b** for **Ni** collector, electrochemical measurement stopped at 0.3 V and was not able to reach the 1.0 V cut-off voltage. Similar to the **SS** current collector, the electrolyte colour was also changed to light blue/green. These behaviours were supported by their CV responses presenting that **SS** and **Ni** are not suitable current collectors for the acidic environment in 1.0 M A lCl_3 electrolyte. Conversely, when **GP** was used, a positive shift in the corrosion potential of **GP** evidences that it acts as a barrier against the oxidizing power of the medium, thus reducing the corrosion tendency (37). Considering the **Ti** current collector, even though there is a slight negative shift in the corrosion potential, the corrosion current as a measure of corrosion rate is lower than the other two current collectors (**SS**, **Ni**).

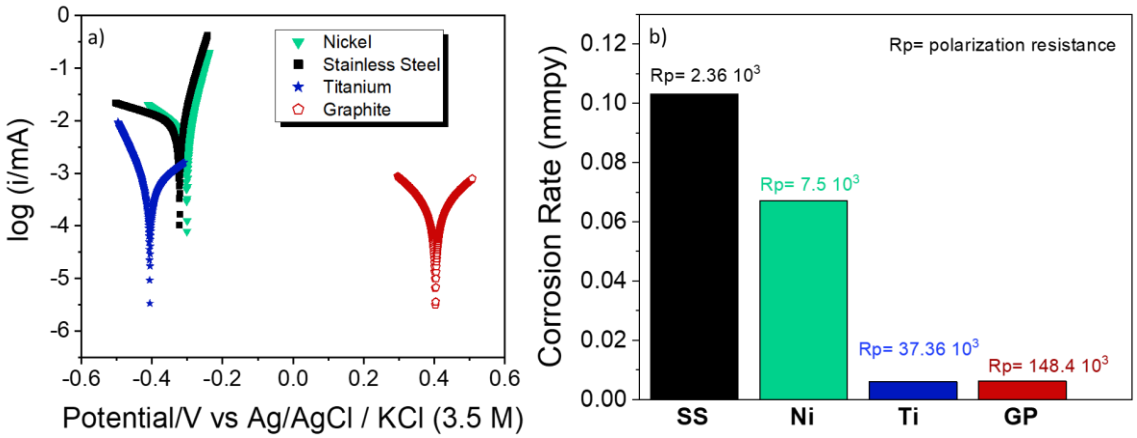

Figure 2. a) Tafel extrapolation fitting curves of current collectors, b) Comparison of corrosion rates and polarization resistances calculated by Eq. (1)

The Stern-Geary equations (Eq. 1-2) describes the relationship between the polarization resistance and the corrosion current (34, 38).

$$B = \frac{\beta a \beta c}{2.303 \times (\beta a + \beta c)} \qquad \text{(Eq. 1)}$$

$$i_{corr.} = \frac{B}{Rp} \quad \text{(Eq. 2)}$$

B term is the Stern-Geary constant, βa is the anodic Tafel constant, βc catodic Tafel constant, Rp is the polarization resistance (ohm cm^{-2}) and $i_{corr.}$ is the corrosion current value (μA cm^{-2}).

The corrosion potential, anodic Tafel constant (β_a), cathodic Tafel constant (β_c), corrosion current and polarization resistance of current the collectors are reported in **Table 1**. The fit of the raw Tafel data was adjusted with EC-Lab software. Anodic, cathodic constants (β_a, β_c), corrosion voltage ($E_{corr.}$) and corrosion current ($i_{corr.}$) values were calculated with equivalent mass and density values given in ASTM standards (ASTM Standards - G102) (39). The corrosion current value, which is a measure of the corrosion rate, was calculated in μA/cm^2 and then converted to the mm per year (mmpy) considering the equivalent weight and density of the corresponding current collector materials (**Table 1**). According to the corrosion rate, **Ti** and **GP** current collectors have low corrosion rates and high polarization resistance, while **Ni** and **SS** have high corrosion rates and very low resistance. As can be clearly seen from **Table 1**, the corrosion current value and therefore the corrosion rate of **GP** is much lower than the others. The corrosion resistance of the graphite current collector is quite high compared to other current collectors, which could be the reason for the low corrosion tendency.

Table 1. Tafel extrapolation fitting corrosion parameters.

	Nickel	**Titanium**	**Stainless Steel**	**Graphite**
β_a (mV)	42.3	259.4	50.3	254.5
β_c (mV)	223.6	74.0	493.3	237.6
$E_{corr.}$ (mV)	-300.817	-403.694	-316.73	403.486
$I_{corr.}$ (μA cm^{-2})	6.481	0.667	8.4	0.360
R_p (Polarization Resistance)	$7.5 \cdot 10^3$	$37.36 \cdot 10^3$	$2.36 \cdot 10^3$	$148.4 \cdot 10^3$
Corrosion rate (mm y^{-1})	0.067	0.0058	0.103	0.0063

In order to further examine the effect of current collectors, TiO_2 electrode was used as a suitable active material for Al-ion batteries (40, 41). The morphological aspects of the TiO_2 sample were investigated by SEM in **Figure 3(a-b)**. According to the SEM images, uniform spherical textures with different sizes can be clearly observed. X-Ray diffraction analysis was performed to determine the crystal structure of TiO_2 synthesized in **Figure 3c**. The diffraction peaks are

positioned at 2θ values of 25°, 38°, 47.8°, 53.9°, 55°, 62.7°, 68° which can be indexed as (101), (004), (200), (105), (204), (220) and (215) crystalline planes of anatase phase TiO_2, (JCPDS No: 21–1272) (19, 31). All these peaks are in agreement with the crystal structure of the pure anatase phase of TiO_2. From Scherrer and Bragg equation, the particle crystal size and (101) plane d-spacing were observed to be around 10.1 nm and 0.349 nm, respectively. From the TEM and HR-TEM images in **Figure 3(d-f)**, it can be observed that TiO_2 was successfully obtained with uniform interconnected spherical nanoparticles, as supported by the SEM images. The selected area electron diffraction (SAED) patterns provided information about the lattice spacing of TiO_2, which was calculated to be about 0.348 nm corresponding to the (101) plane. Moreover, the SAED patterns show that the TiO_2 anatase phase is represented by the planes (101), (004), (200), (105), (204), (220), referring to the crystal structure of the Miller Index as given in **Table S1.**

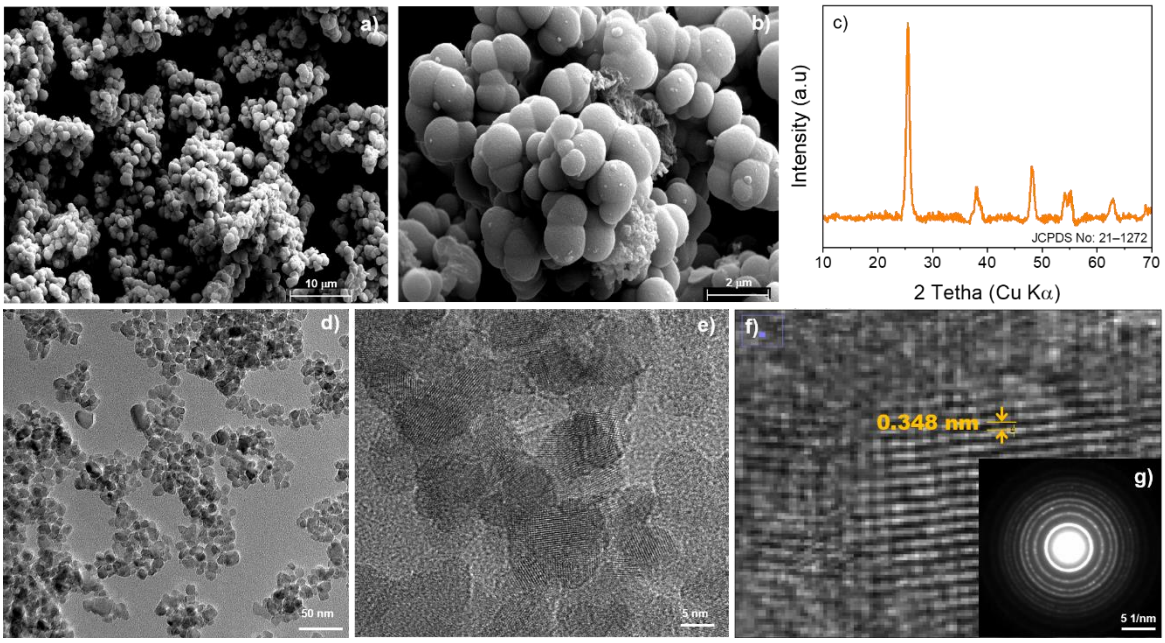

Figure 3. SEM images of synthesized anatase TiO_2, a, b) at different display sizes, c) X-ray diffraction pattern of synthesized anatase phase of TiO_2, d, e, f) TEM, HR-TEM, g) SAED (selected area electron diffraction) analysis of synthesized anatase TiO_2.

Galvanostatic charge-discharge performances and cyclic voltammetry experiments were performed in a 3-electrode system in 1.0 M $AlCl_3$ aqueous electrolyte at a scan rate of 5 mV s^{-1} with a graphite counter electrode and Ag/AgCl reference electrode. The voltage (V) vs current (mA/cm^2) curves of TiO_2 coated on different current collectors are shown in **Figure 4**. The

reduction and oxidation peaks at approximately (-1.06 and -1.02) V and (-1.06 and -0.98) V, respectively, can be observed with **GP** electrode and the peaks can typically result from Al^{3+} ion and/or proton insertion depending on the acidity of the electrolyte (42, 43). The effect of proton insertion on the charge storage mechanism at different pH values is beyond the scope of this study. Regarding the **Ti** current collector, no redox peaks were detected for the TiO_2 electrode on **Ti**, since the operating voltage was not able to go into the more negative voltage range. Looking again at the CV plots presented in **Figure 1**, it can be seen that the bare **Ti** current collector cannot go further down to negative voltage and hydrolysis of water starts after about (-0.5 V), which is supported by the sharp drop in current values. The tests of TiO_2 on **SS** and **Ni** (**Figure 4c**, **d**) showed a similar trend to the CV measurements obtained with the bare current collectors (**Figure 1**), the system was able to operate for 2 cycles and then stopped cycling due to intense H_2 outgassing.

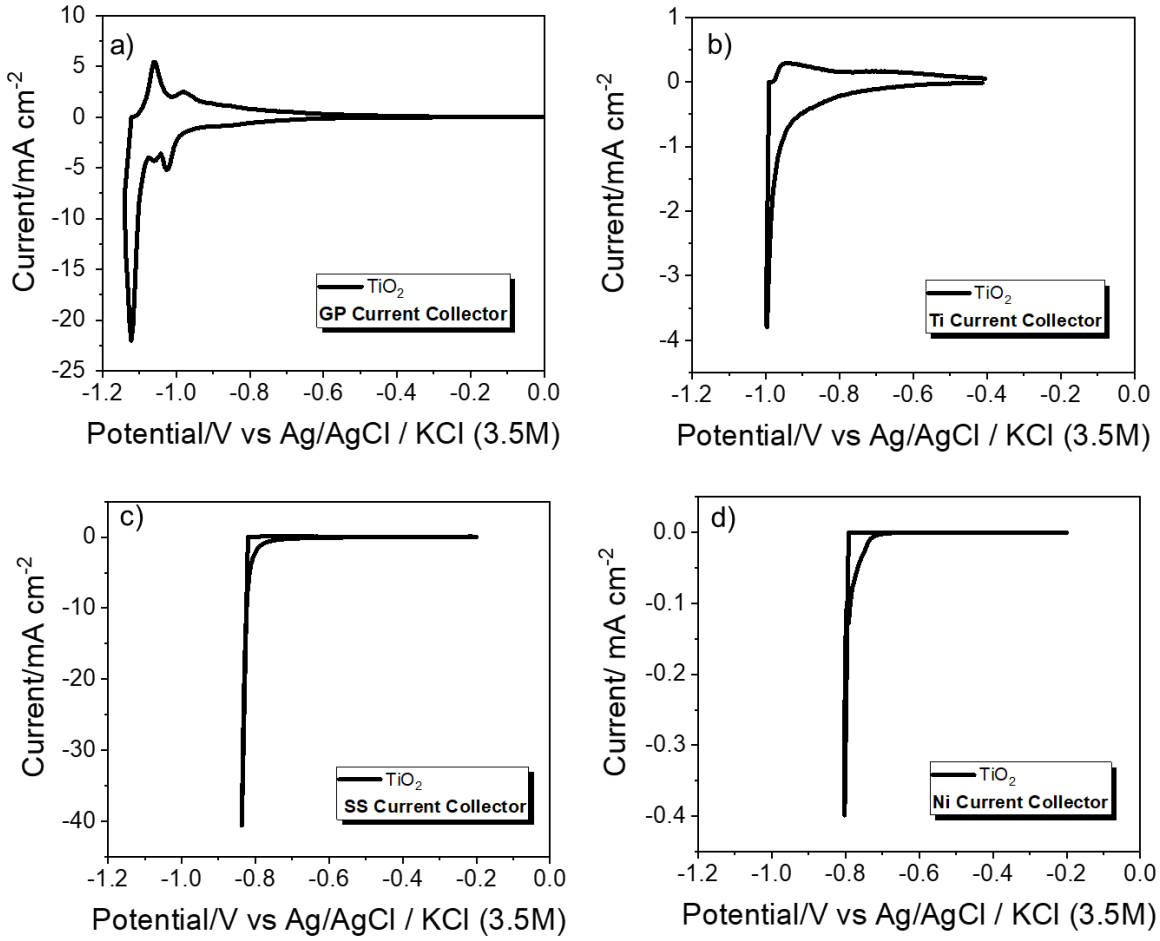

Figure 4. Cyclic voltammetry (CV) curves of synthesized anatase TiO_2 on a) **GP**, b) **Ti**, c) **SS**, e) **Ni** current collectors.

The galvanostatic charge-discharge specific capacity performances and Coulombic efficiency of TiO_2 deposited on the **GP** current collector are shown in **Figure 5**. Electrochemical performances were performed in a 3-electrode cell arrangement at a current density of 3 A/g with 1.0 M $AlCl_3$. In **Figure 5a**, the C-rate performance of TiO_2 on GP was tested over a voltage range of (-1.13 and -0.2) V for 10 cycles low current density (3 A g^{-1}) to higher current density (20 A g^{-1}). The first discharge capacity value was around 288 mAh g^{-1} at a current density of 3 A g^{-1} and the capacities were dropped upon testing at higher current rates over 50 cycles. After C-rate measurement, longer cycle performance was tested at the current of 3 A g^{-1} (**Figure 5b**). An initial discharge capacity of 249 mAh g^{-1} was achieved, which dropped to a discharge capacity of 105 mAh g^{-1} over 50 cycles, with a Coulombic efficiency of 73.9 %. As can be observed, aqueous electrolyte Al-ion batteries with TiO_2 electrodes suffer from low Coulombic efficiency, which is also addressed in other studies in the literature (19, 44, 45). The main reasons for the low Coulombic efficiency can be explained as the formation of H_2 as a side reaction on the current collectors and the irreversible reduction of Ti^{4+} cation to Ti^{2+} during the charging process (45). No specific capacities were achieved with the **SS** and **Ni** current collectors during the galvanostatic charge-discharge performances while a poor electrochemical activity was obtained on **Ti** and H_2 formation was observed as the voltages decreased to negative values (**Figure S4**). When the current collectors were photographed after galvanostatic charge-discharge tests (**Figure S5**), **Ti** and **GP** current collectors remained unchanged, while **SS** and **Ni** showed significant degradation. The corrosion parameters of TiO_2 containing **GP** and **Ti** current collectors before and after 50 cycles were also compared. **Figure S6** shows that the corrosion voltages in both TiO_2 containing current collectors are shifted to the left, which means that the resistance to the oxidizing power of the environment to form a barrier decreases as the cycling increases (37). When the corrosion current values were analyzed, an increase was observed at the 50^{th} cycle compared to the pre-cycle corrosion currents, indicating an increased tendency of the electrodes to corrode during cycling. **Table S2** shows the comparison of corrosion parameters for **GP** and **Ti** current collectors. There is an increase in the corrosion current values as a result of the cycling, but the corrosion current of the **GP** current collector after cycling is still small compared to **Ti**. It means that **GP** corrosion resistance is greater than that of the **Ti** current collector. As a whole, the present study confirms that synthesized TiO_2 electrode is a promising anode material for AAIBs, in comparison to recent studies on the electrochemical performances of TiO_2 electrodes in aqueous electrolyte Al-ion batteries (**Table S3**). Moreover, the current collector's significant effect on the cell performances is

systematically investigated, where the graphite plate outperformed the other **Ti**, **Ni** and **SS** current collectors.

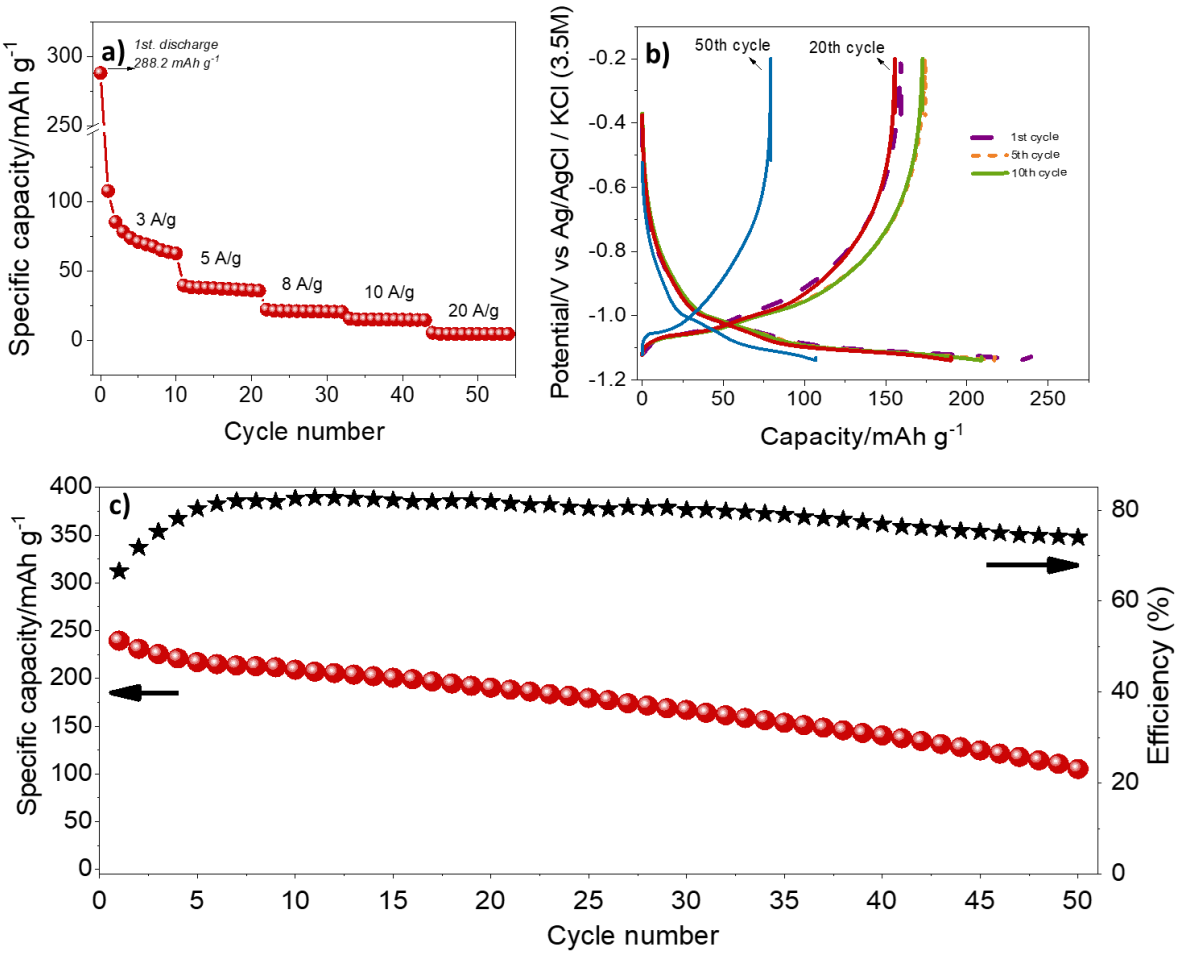

Figure 5. Electrochemical tests of TiO_2 on **GP** current collector a) C-rate tests and b) galvanostatic charge-discharge curves and c) long term cycling and Coulombic efficiency cycled in 1.0 M $AlCl_3$ at 3 A g^{-1}.

4. Conclusion

In this study, the electrochemical performance and corrosion behaviour of current collectors for aqueous electrolyte Al-based energy storage systems were investigated. Corrosion tests, CV measurements and galvanostatic charge-discharge performances have shown that current collectors have an important place to improve the electrochemical performance of AAIBs. The electrochemical behaviour of **SS**, **Ni**, **Ti** and **GP** current collectors was first determined by CV. Second, corrosion behaviours were investigated with LPR using Tafel extrapolation method. To evidence clearly the effect of the current collectors, TiO_2 active material, synthesized by a

sol-gel method, was employed as an electrode material on four different types of current collectors. Overall, through corrosion tests, cyclic voltammetry and charge-discharge studies, **GP** is proven to be a favourable choice by minimizing the corrosion effect and HER. Finally, the TiO_2 electrode on **GP** current collector provides a discharge capacity of 249 mAh g^{-1}, while **Ti** current collector resulted in a less significant electrochemical activity. Conversely, the use of **SS** and **Ni** current collectors were reported to be unsuitable for AAIBs due to their corrosion tendencies and low electrochemical stability.

Acknowledgements

Burcu Unal acknowledges the 100/2000 Doctoral Fellowship Program of the Turkish Higher Education Council (YÖK) and the 2211/C National Doctoral Fellowship Program for Priority Areas in Science of the Scientific and Technological Research Council of Turkey (TÜBİTAK). This work is part of Burcu Unal's PhD thesis.

References

1. Melzack N, Wills RGA, Cruden A. (2021) Cleaner Energy Storage: Cradle-to-Gate Life Cycle Assessment of Aluminum-Ion Batteries With an Aqueous Electrolyte. Front Energy Res. 9: 699919
2. Wu D, Li X, Liu X, Yi J, Acevedo-Peña P, Reguera E, et al. (2022) 2022 Roadmap on aqueous batteries. JPhys Energy. 2022;4(4).
3. Eftekhari A, Corrochano P. (2017) Electrochemical energy storage by aluminum as a lightweight and cheap anode/charge carrier. Sustainable Energy & Fuels. 1(6):1246-64.
4. Sun H, Wang W, Yu Z, Yuan Y, Wang S, Jiao S. (2015) A new aluminium-ion battery with high voltage, high safety and low cost. Chem Commun. 51(59):11892-5.
5. Ambroz F, Macdonald TJ, Nann T. (2017) Trends in Aluminium-Based Intercalation Batteries. Advanced Energy Materials. 7(15):1602093.
6. Smith BD, Wills RGA, Cruden AJ. (2020) Aqueous Al-ion cells and supercapacitors — A comparison. Energy Reports. 6:166-73.
7. Yuan D, Zhao J, Manalastas W, Kumar S, Srinivasan M. (2020) Emerging rechargeable aqueous aluminum ion battery: Status, challenges, and outlooks. Nano Materials Science. 2(3):248-63.
8. Jayaprakash N, Das SK, Archer LA. (2011) The rechargeable aluminum-ion battery. Chem Commun. 47(47):12610-2.
9. Lin M-C, Gong M, Lu B, Wu Y, Wang D-Y, Guan M, et al. (2015) An ultrafast rechargeable aluminium-ion battery. Nature. 520(7547):324-8.
10. Holland A, McKerracher RD, Cruden A, Wills RGA. (2018) An aluminium battery operating with an aqueous electrolyte. Journal of Applied Electrochemistry. 48(3):243-50.
11. Ru Y, Zheng S, Xue H, Pang H. (2019) Different positive electrode materials in organic and aqueous systems for aluminium ion batteries. Journal of Materials Chemistry A. 7(24):14391-418.
12. Demir-Cakan R, Palacin MR, Croguennec L. (2019) Rechargeable aqueous electrolyte batteries: from univalent to multivalent cation chemistry. Journal of Materials Chemistry A. 7(36):20519-39.

13. Pan W, Wang Y, Zhang Y, Kwok HYH, Wu M, Zhao X, et al. (2019) A low-cost and dendrite-free rechargeable aluminium-ion battery with superior performance. Journal of Materials Chemistry A. 7(29):17420-5.
14. Cheng Y, Liu T, Shao Y, Engelhard MH, Liu J, Li G. (2014) Electrochemically stable cathode current collectors for rechargeable magnesium batteries. J Mater Chem A.;2(8):2473-7.
15. Verma V, Kumar S, Manalastas W, Satish R, Srinivasan M. (2019) Progress in Rechargeable Aqueous Zinc- and Aluminum-Ion Battery Electrodes: Challenges and Outlook. Advanced Sustainable Systems. 3(1):1800111.
16. Liu Y, Sang S, Wu Q, Lu Z, Liu K, Liu H. (2014) The electrochemical behavior of Cl^- assisted Al^{3+} insertion into titanium dioxide nanotube arrays in aqueous solution for aluminum ion batteries. Electrochimica Acta. 143:340-6.
17. Kumar S, Rama P, Yang G, Lieu WY, Chinnadurai D, Seh ZW. (2022) Additive-Driven Interfacial Engineering of Aluminum Metal Anode for Ultralong Cycling Life. Nano-Micro Letters. 15(1):21.
18. Wang H, Bai Y, Chen S, Luo X, Wu C, Wu F, et al. (2015) Binder-free V_2O_5 cathode for greener rechargeable aluminum battery. ACS Appl Mater Interfaces. 7(1):80-4.
19. Liu S, Hu JJ, Yan NF, Pan GL, Li GR, Gao XP. (2012) Aluminum storage behavior of anatase TiO_2 nanotube arrays in aqueous solution for aluminum ion batteries. Energy & Environmental Science. 5(12):9743.
20. Kazazi M, Abdollahi P, Mirzaei-Moghadam M. (2017) High surface area TiO_2 nanospheres as a high-rate anode material for aqueous aluminium-ion batteries. Solid State Ionics. 300:32-7.
21. Holland A, McKerracher R, Cruden A, Wills R. (2018) Electrochemically Treated TiO_2 for Enhanced Performance in Aqueous Al-Ion Batteries. Materials (Basel). 11(11):2-12.
22. Nandi S, Das SK. (2019) Realizing a Low-Cost and Sustainable Rechargeable Aqueous Aluminum-Metal Battery with Exfoliated Graphite Cathode. ACS Sustainable Chemistry & Engineering. 7(24):19839-47.
23. Rani JV, Kanakaiah V, Dadmal T, Rao MS, Bhavanarushi S. (2013) Fluorinated Natural Graphite Cathode for Rechargeable Ionic Liquid Based Aluminum–Ion Battery. Journal of The Electrochemical Society. 160(10):A1781.
24. Liu S, Pan GL, Li GR, Gao XP. (2015) Copper hexacyanoferrate nanoparticles as cathode material for aqueous Al-ion batteries. Journal of Materials Chemistry A. 3(3):959-62.
25. Vujković MJ, Etinski M, Vasić B, Kuzmanović B, Bajuk-Bogdanović D, Dominko R, et al. (2021) Polyaniline as a charge storage material in an aqueous aluminum-based electrolyte: Can aluminum ions play the role of protons? Journal of Power Sources. 482:228937.
26. Sariyer S, Ghosh A, Dambasan SN, Halim EM, El Rhazi M, Perrot H, et al. (2022) Aqueous Multivalent Charge Storage Mechanism in Aromatic Diamine-Based Organic Electrodes. ACS Applied Materials & Interfaces. 14(6):8508-20.
27. Yan L, Zeng X, Zhao S, Jiang W, Li Z, Gao X, et al. (2021) 9,10-Anthraquinone/K(2)CuFe(CN)(6): A Highly Compatible Aqueous Aluminum-Ion Full-Battery Configuration. ACS Appl Mater Interfaces. 13(7):8353-60.
28. Reed LD, Menke E. (2013) The Roles of V_2O_5 and Stainless Steel in Rechargeable Al–Ion Batteries. Journal of The Electrochemical Society. 160(6):A915.
29. Oh Y, Lee G, Tak Y. (2018) Stability of Metallic Current Collectors in Acidic Ionic Liquid for Rechargeable Aluminum-Ion Batteries. ChemElectroChem. 5(22):3348-52.
30. Lahan H, Das SK. (2018) Active role of inactive current collector in aqueous aluminum-ion battery. Ionics. 24(7):2175-80.
31. Lahan H, Das SK. (2019) Al^{3+} ion intercalation in MoO3 for aqueous aluminum-ion battery. Journal of Power Sources. 413:134-8.
32. Sang S, Liu Y, Zhong W, Liu K, Liu H, Wu Q. (2016) The electrochemical behavior of TiO_2-NTAs electrode in H^+ and Al^{3+} coexistent aqueous solution. Electrochimica Acta. 187:92-7.
33. Kim YS, Kriegel S, Harris KD, Costentin C, Limoges B, Balland V. (2017) Evidencing Fast, Massive, and Reversible H^+ Insertion in Nanostructured TiO_2 Electrodes at Neutral pH. Where Do Protons Come From? The Journal of Physical Chemistry C. 121(19):10325-35.

34. Revie R, Wau HH. (2008) Corrosion and Corrosion Control. An Introduction to Corrosion Science and Engineering. 4 ed. New Jersey, John Wiley & Sons.
35. Li W, Cochell T, Manthiram A. (2013) Activation of Aluminum as an Effective Reducing Agent by Pitting Corrosion for Wet-chemical Synthesis. Scientific Reports. 3(1):1229.
36. Akpanyung KV, Loto RT. (2019) Pitting corrosion evaluation: a review. Journal of Physics: Conference Series. 1378(2):022088.
37. Raza MA, Ali A, Ghauri FA, Aslam A, Yaqoob K, Wasay A, et al. (2017) Electrochemical behavior of graphene coatings deposited on copper metal by electrophoretic deposition and chemical vapor deposition. Surface and Coatings Technology. 332:112-9.
38. McCafferty E. (2009) Introduction to Corrosion Science. USA, Springer Science.
39. ASTM (Reapproved 1999) Standard Practice for Calculation of Corrosion Rates and Related Information from Electrochemical Measurements. ASTM Standards G102-89: Annual Book of International ASTM Standards.
40. Das SK, Palaniselvam T, Adelhelm P. (2019) Electrochemical study on the rechargeability of TiO_2 as electrode material for Al-ion batteries with chloroaluminate ionic liquid electrolyte. Solid State Ionics. 340:115017.
41. Auer A, Kunze-Liebhäuser J. (2019) Recent Progress in Understanding Ion Storage in Self-Organized Anodic TiO_2 Nanotubes. Small Methods. 3(8):1800385.
42. Kim YS, Balland V, Limoges B, Costentin C. (2017) Cyclic voltammetry modeling of proton transport effects on redox charge storage in conductive materials: application to a TiO_2 mesoporous film. Phys Chem Chem Phys. 19(27):17944-51.
43. Makivić N, Cho JY, Harris KD, Tarascon JM, Limoges B, Balland V. (2021) Evidence of Bulk Proton Insertion in Nanostructured Anatase and Amorphous TiO_2 Electrodes. Chemistry of Materials. 33(9):3436-48.
44. Lahan H, Das SK. (2018) An approach to improve the Al^{3+} ion intercalation in anatase TiO_2 nanoparticle for aqueous aluminum-ion battery. Ionics. 24(6):1855-60.
45. Wu X, Qin N, Wang F, Li Z, Qin J, Huang G, et al. (2021) Reversible aluminum ion storage mechanism in Ti-deficient rutile titanium dioxide anode for aqueous aluminum-ion batteries. Energy Storage Materials. 37:619-27.

SUPPORTING INFORMATION

Current Collectors Corrosion Behaviours and Rechargeability of TiO_2 in Aqueous Electrolyte Aluminium-ion Batteries

Burcu Unal[a,b], *Ozlem Sel*[c,d] *and Rezan Demir-Cakan*[a,b*]

[a] Department of Chemical Engineering, Gebze Technical University, Gebze, Kocaeli, 41400, Turkey

[b] Institute of Nanotechnology, Gebze Technical University, Gebze, Kocaeli, 41400, Turkey

[c] Chimie du Solide et de l'Energie, UMR 8260, Collège de France, 11 Place Marcelin Berthelot, 75231 Paris Cedex 05, France

[d] Réseau sur le Stockage Electrochimique de l'Energie (RS2E), CNRS FR 3459, 33 Rue Saint Leu, 80039 Amiens Cedex, France

*Corresponding author: demir-cakan@gtu.edu.tr

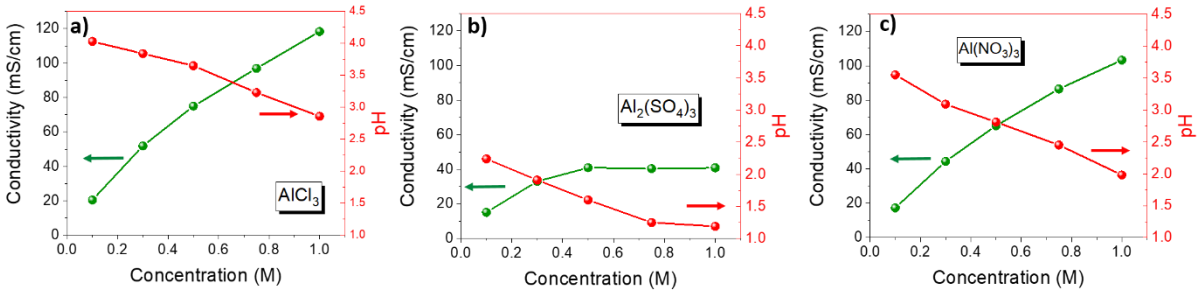

Figure S1. pH and ionic conductivities of a) $AlCl_3$, b) $Al_2(SO_4)_3$ and c) $Al(NO_3)_3$ aqueous electrolytes at different concentrations.

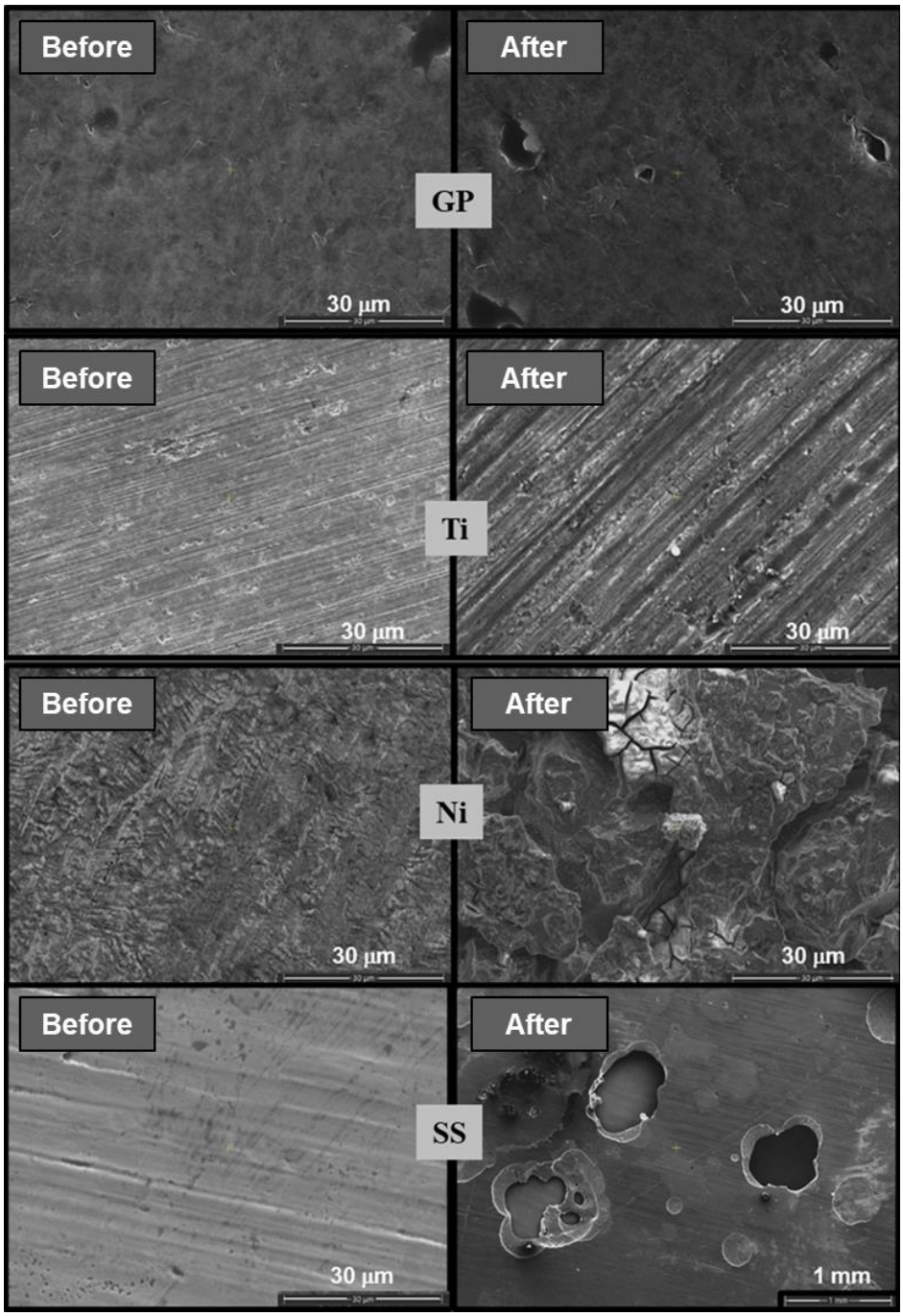

Figure S2. SEM images of current collectors, before and after CV measurements in 1.0 M $AlCl_3$: **GP**, **Ti**, **Ni**, **SS** (from up to down, respectively).

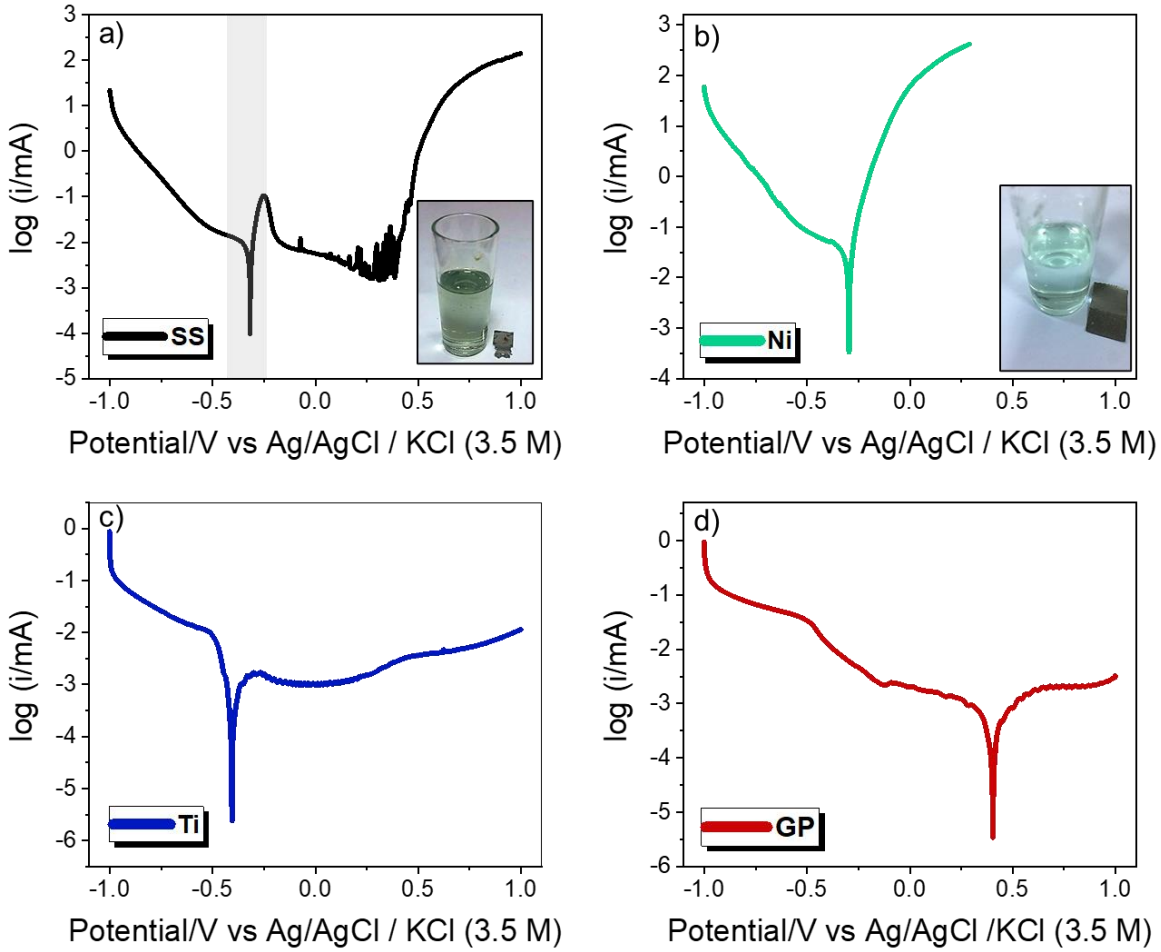

Figure S3. Potentiodynamic polarization curves between (-1.0 – 1.0) V at 1mV s^{-1} scan rate in 1.0 M $AlCl_3$. a) **SS**, b) **Ni**, c) **Ti**, d) **GP**.

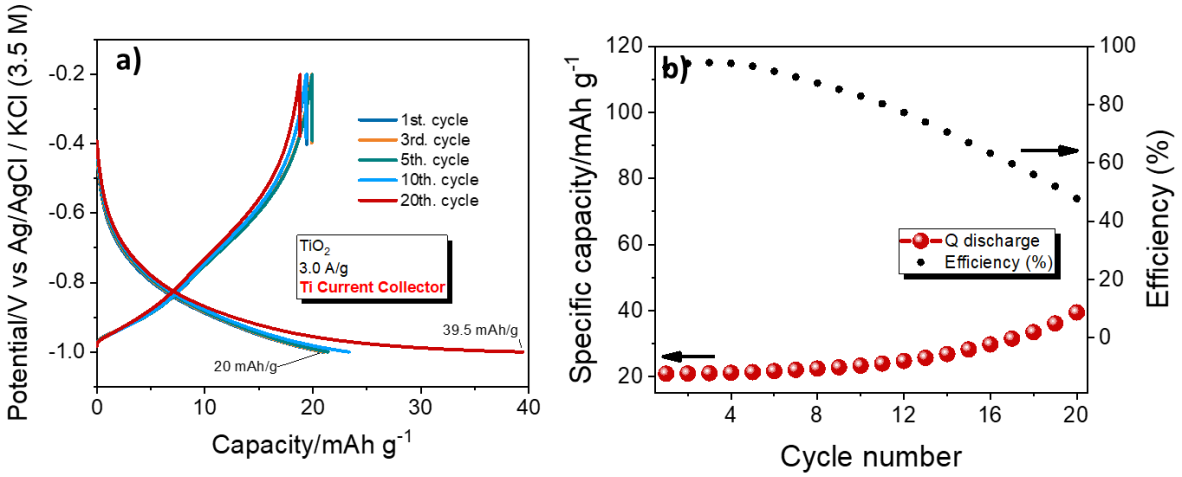

Figure S4. Electrochemical test of TiO_2 on **Ti** current collector cycled in 1.0 M $AlCl_3$ containing aqueous electrolyte at 3A g^{-1} a) galvanostatic charge-discharge curves and b) capacity retention profile

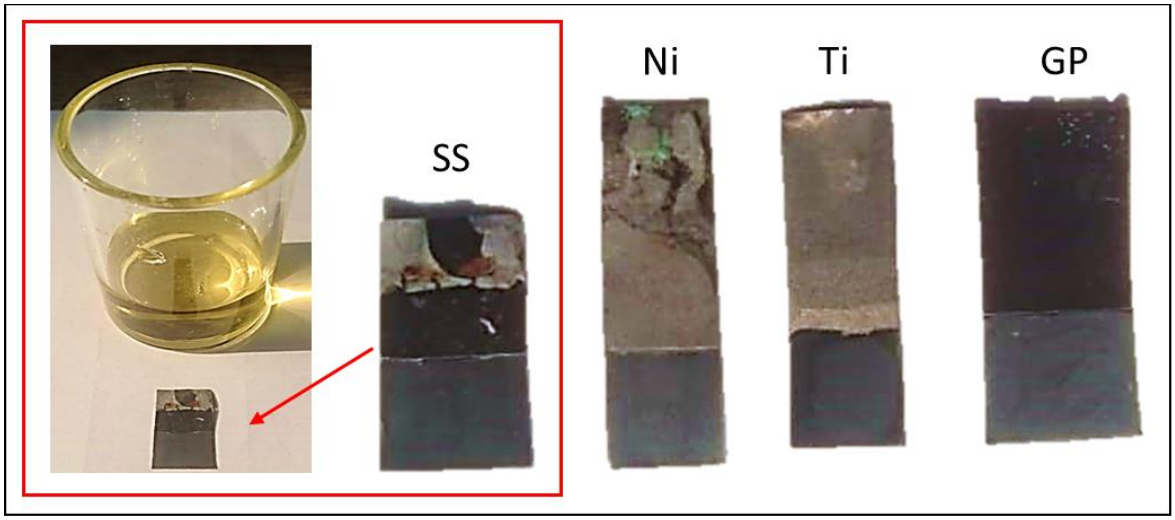

Figure S5. Images of TiO_2 coated **SS**, **Ni**, **Ti** and **GP** current collectors demonstrating the macroscopic changes in electrolyte after galvanostatic charge-discharge experiment in 1.0 M $AlCl_3$ containing aqueous electrolyte.

Table S1. Lattice spaces attributed to the Miller Index of anatase TiO_2 from selected area electron diffraction (SAED).

	1/2r (nm^{-1})	1/r (nm^{-1})	r (nm)	d-space (Å)	Miller Index (hkl)
1	5.973	2.987	0.335	3.348	101
2	8.441	4.221	0.237	2.369	004
3	10.621	5.311	0.188	1.883	200
4	11.928	5.964	0.168	1.677	105
5	13.605	6.803	0.147	1.470	204
6	14.982	7.491	0.133	1.335	220

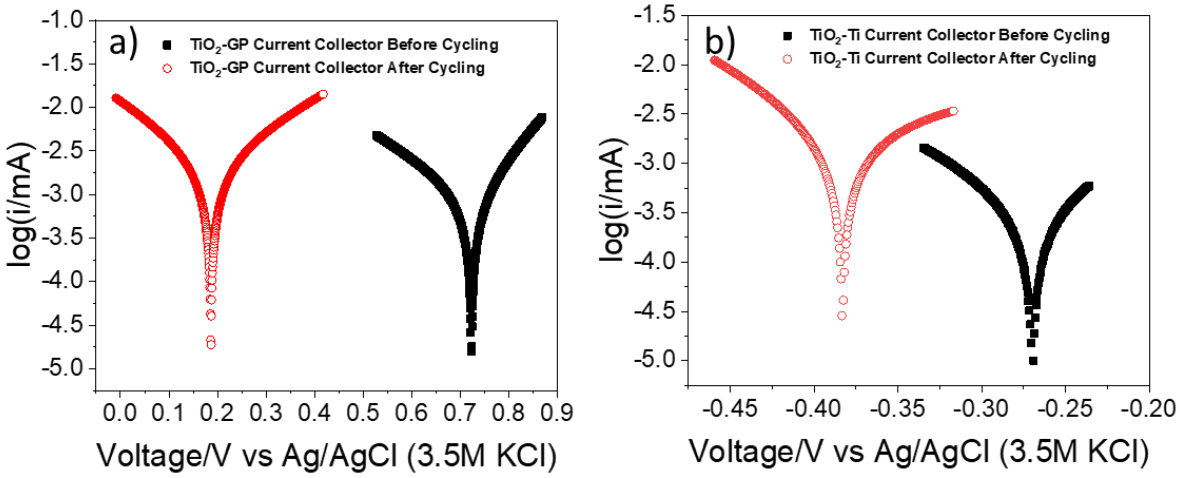

Figure S6. Tafel extrapolation fitting curves of TiO_2 containing **Ti** and **GP** current collectors, a) TiO_2 containing GP current collector before/after cycling b) TiO_2 containing **Ti** current collector before/after cycling.

Table S2. Tafel extrapolation fitting corrosion parameters of TiO_2 containing **GP** and **Ti** current collectors at before/after cycling.

	Ti before cycle	Ti after 50th cycle	GP before cycle	GP after 50th cycle
βa (mV)	133.1	448.7	163.7	314.8
βc (mV)	122.6	119.5	291.0	290.2
$E_{corr.}$ (mV)	-270	-383	723	186
$I_{corr.}$ (µA cm^{-2})	0.472	3.03	1.02	2.70
R_p (Polarization Resistance)	$58.7 \cdot 10^3$	$13.5 \cdot 10^3$	$44.65 \cdot 10^3$	$24.31 \cdot 10^3$

Table S3. An electrochemical performance comparison of TiO_2 electrodes for aqueous electrolyte Al-ion batteries.

Electrode	Electrolyte	Current Collector	Current Density	Discharge Capacity	Efficiency (%)	Ref.
Anodic treated TiO_2-NTA	0.25 M $Al_2(SO_4)_3$ 1.5 M NaCl mixed soln.	Ti foil	4mA cm^{-2}	74.5 mAh g^{-1}	N/A	(15)
TiO_2, anatase nanotube	1.0 M $AlCl_3$	Ti foil	4mA cm^{-2}	75 mAh g^{-1} (14 cycles)	N/A	(18)
Treated-TiO_2	1.0 M $AlCl_3$/1.0 M KCl	Carbon polymer	0.2 - 10 A g^{-1} (various current densities)	23.1 mAh g^{-1} (60 cycles at 1.0 A g^{-1}) 15.3 mAh g^{-1} at 10 A g^{-1}	96.2 99.95	(20)
TiO_2-NSs	1.0 M $AlCl_3$	Nickel disks	0.15C and 6.0C	183 mAh g^{-1} at 0.15C (initial capacity) 108 mAh g^{-1} at 6.0 C (initial)	N/A	(19)
TiO_2/CNT	1.0 M $AlCl_3$	Nickel disks	1C (335 mA g^{-1})	170 mAh g^{-1} (100 cycles)	99.9	(29)
TiO_2, anatase	1.0 M $AlCl_3$	Graphite Ti foil	4A g^{-1}	140 mAh g^{-1} (20 cycles) 35 mAh g^{-1} (30 cycles)	~48 ~50	(43)
Ti-deficient rutile TiO_2	1.0 M $AlCl_3$/1.0 M NaCl	Tantalum foil	3A g^{-1}	64 mAh g^{-1} (110 cycles)	~50	(44)
TiO_2, anatase	1.0 M $AlCl_3$	Graphite plate	3 A g^{-1}	249 mAh g^{-1} (initial) 105 mAh g^{-1} (50 cycles)	~73.9	Present work